Chapter

Janus Nanosheets Derived from $K_4Nb_6O_{17}{\cdot}3H_2O$ *via* Regioselective Interlayer Surface Modification

Ryoko Suzuki, Mitsuhito Sudo, Megumi Hirano, Naokazu Idota, Masashi Kunitake, Taisei Nishimi and Yoshiyuki Sugahara

Abstract

Inorganic Janus nanosheets were successfully prepared using the difference in reactivity between interlayers I and II of layered hexaniobate $K_4Nb6O_{17}{\cdot}3H_2O$. Janus nanosheets exhibit the highest anisotropy among Janus compounds due to their morphology. It is therefore important to prepare Janus nanosheets with stable shapes in various solvents, robust chemical bonds between nanosheets and fuctional groups and high versatility due to surface functional groups. $K_4Nb_6O_{17}{\cdot}3H_2O$, which possesses two types of interlayers and two types of organophosphonic acids that react with metal oxides to form robust covalent bonds, was employed to prepare Janus nanosheets for this study. Interlayer I was modified by octadecylphosphonic acid, followed by modification by carboxypropylphosphonic acid mainly at interlayer II. Preparation of Janus nanosheets with two organophosphonate moieties was confirmed by ^{31}P MAS NMR. After these regioselective and sequential modifications, the products were exfoliated into single-layered nanosheets in THF. Two types of derivatives with different repeating distances were recovered from a dispersion containing nanosheets exfoliated by different processes, centrifugation, and solvent evaporation. AFM analysis of the exfoliated nanosheets revealed that the products were Janus compounds. There are high expectations for application of these types of Janus nanosheets in various fields and for design of various Janus nanosheets using this preparation method.

Keywords: Janus nanosheets, $K_4Nb_6O_{17}{\cdot}3H_2O$, organophosphonic acid, grafting reaction, intercalation

1. Introduction

A Janus compound has two surface properties, and each of these properties appears on one of two sides of the compound [1]. Janus compounds are expected to be applied as functional materials, including electronic paper [2], solid surfactants [3], optics materials [4], and drug delivery system (DDS) vectors [5]. The morphology of Janus compounds is classified into three categories: 0-dimensional compounds such as particles; one-dimensional compounds including cylinders, tubes, and rods; and two-dimensional compounds, typically sheets or discs [6–10].

There are various methods of preparing Janus nanoparticles. Regioselective surface modification of nanoparticles can produce Janus nanoparticles [11]. By forming nanoparticles with two raw materials, Janus nanoparticles with different compositions can be prepared [2]. Self-assembly and subsequent cross-linking of polymer chains can also produce Janus nanoparticles [12]. Janus rods can be prepared by forming silica using TEOS by the sol-gel method on Fe_3O_4 regioselectively [13]. Janus cylinders can be prepared by masking one side of a cylinder and conducting subsequent modification of the other side [14].

Janus nanosheets exhibit the highest anisotropy among Janus compounds due to their unique morphology. They are also useful as emulsifiers, because Janus nanosheets cannot rotate at the interfaces of micelles [15]. Most Janus nanosheets reported so far have consisted of polymers. Stupp et al. reported the preparation of Janus nanosheets by polymerization of oligomers with polymerizable groups [16]. Polymerization of oligomers led to the formation of sheet morphology, because the polymerizable groups were located at the center of an oligomer. Walther et al. used triblock copolymers, polystyrene-*block*-polybutadiene-*block*-poly(*tert*-butyl methacrylate), for preparing Janus nanosheets [17]. Janus nanosheets were prepared by cross-linking polybutadiene domains of the triblock copolymers, and the resulting Janus nanosheets had two types of surfaces, polystyrene, and poly(*tert*-butyl methacrylate) moieties. These methods are based on selective polymerization or cross-linking. On the other hand, Janus nanosheets were prepared by dropping poly(ε-caprolactone) at the interface between water and pentyl acetate and evaporating solvents to crystallize polymers [10]. The properties of Janus compounds were realized by folding the polymer an odd number of times, which exposed carboxyl groups on one side of the nanosheets. Although polymer-based Janus nanosheets have been prepared, these Janus nanosheets became swollen and deformed in organic solvents because they were composed of polymers [18].

It is therefore obvious that the preparation of inorganic Janus nanosheets is an important issue. There are only a few reports of preparation of Janus nanosheets derived from inorganic compounds, however, comprising silica nanosheets prepared by the sol-gel method [19–21] and fluorohectorite, which is a layered clay mineral [22].

Silica-based Janus nanosheets were prepared by hydrolysis and condensation of two trifunctional organoalkoxysilanes. First, phenylalkoxysilane was assembled on the surface of oil in a W/O emulsion and reacted by the sol-gel method. The product, which formed a hollow shell, was further reacted with aminoalkyltrialkoxysilane. The resultant product had phenyl groups and amino groups on the inner and outer surfaces of hollow particles, respectively. Janus nanosheets were obtained by breaking the hollow silica particles using a colloid milling method. The resulting Janus nanosheets have a thickness of 65 nm and a curvature originating from the hollow particle morphology [19]. Another method of preparing silica-based Janus nanosheets using a $CaCO_3$ template was also reported. First, 3-butyldianhydride mercaptopropyltrimethoxysilane was assembled on the surface of $CaCO_3$ particles and reacted using a sol-gel process. The products were further reacted with octadecyltrichlorosilane. Janus nanosheets were obtained by removing the templates and crushing the resultant hollow particles. Janus nanosheets with single a nanometer thickness were prepared by this method [21]. These sol-gel preparation methods, which were developed by Yang et al., required adsorption of organosilanes on liquid-liquid interfaces or self-assembly on templates. Thus, these methods restricted the reaction system design and choices of molecules.

Another method of preparing Janus nanosheets using inorganic layered material was reported in which the Janus nanosheets consisted of a sheet of a clay mineral, fluorohectorite, and two cationic polymers. The interlayer of fluorohectorite was selectively exfoliated into double-layered nanosheets. Both surfaces of the products, which had a negative charge, were modified with a cationic polymer, protonated polyethyleneimine-ethylene oxide. After that, the products were exfoliated into single-layered nanosheets, and one surface which had not been modified was reacted with another cationic polymer, protonated dendritic poly(amidoamine). The products had one cationic polymer on one side and the other polymer on the other side of the nanosheets [22]. This preparation method has the advantage that any cationic compound could be used as the modifier, regardless of its functional group. On the other hand, the products use in water was restricted due to the presence of ionic bonds between the surfaces of the clay sheets and the polymers.

Preparation of graphene-based Janus nanosheets has also been developed [23]. For example, two-step functionalization was carried in one report [24]. First, the graphene surface of the substrate was functionalized by a photochlorination reaction. The functionalized graphene was then peeled off the substrate to expose the unmodified side using PMMA film as a mediator. The exposed fresh side of the graphene was further functionalized by phenylation reaction. Graphene-based Janus nanosheets were also prepared using a Pickering emulsion [25]. A graphene oxide (GO) dispersion was mixed with hydrochloric acid and wax, and this mixture was ultrasonicated to prepare a Pickering emulsion. The micelles were then washed with a sodium hydroxide aqueous solution, and GO was adsorbed on the surface of micelles to form a monolayer. The exposed GO surface of the micelles was further modified with alkylamine. Finally, Janus nanosheets were obtained by dissolving wax in chloroform. In the preparation of graphene-based Janus nanosheets, it is necessary that a single layer of graphene be adsorbed on a substrate or at the liquid-liquid interphase to achieve regioselective functionalization.

These earlier studies show that the following conditions are desirable: nanosheets should have covalent bonds with organic groups, the choice of functional groups should not be limited, and regioselective surface modification should be easily achieved. Another preparation method that satisfies the above conditions should therefore be developed.

Some inorganic layered materials have structures in which negatively charged nanosheets and metal cations are piled up alternately. Nanosheets are very thin, just a few atoms thick. On the other hand, their lateral sizes are large, possibly on a micrometer scale. Therefore, these materials have high aspect ratios. From the viewpoints of structure and composition, inorganic layered materials are classified into several categories, including clay minerals [26–28], layered silicate [29–31], and layered transition metal oxide [32–34]. These inorganic layered materials have been used as hosts for inorganic-organic hybrids. There are only two types of reaction for preparing inorganic-organic hybrids: intercalation reactions forming noncovalent bonds and grafting reactions forming covalent bonds. Grafting reactions that form covalent bonds between layer surfaces and organic groups utilize alcohols, carboxylic acids, silane coupling agents, and phosphorous coupling reagents such as organophosphonic acids as modifiers. Grafted organophosphonate moieties, in particular, are seldom eliminated from nanosheet surfaces because organophosphonate moieties form stable M−O−P bonds with nanosheet surfaces, except for Si−O−P bonds, which are known to become hydrolyzed under certain conditions [35]. Surface modification with monolayer can be easily achieved, moreover because homocondensation reactions do not occur between organophosphonic acids under mild conditions [36]. There have been many reports of surface modification by silane coupling agents for clay minerals [37], layered silicates [38–40], and layered transition metal oxides [41, 42]. In the case of surface modification by alcohol, there have been reports of polysilicates with ethylene glycol [43] and aliphatic alcohols [44], while layered perovskites have been modified with *n*-alcohol [45] and alcohol with fluoroalkyl groups [44, 46]. Also, layered perovskites were grafted with phenyl or *n*-alkylphosphonic acids using the aforementioned *n*-alkoxy derivatives as intermediates [47].

Layered hexaniobate ($K_4Nb_6O_{17}{\cdot}3H_2O$) has a unique structure among layered transition metal oxides; $K_4Nb_6O_{17}{\cdot}3H_2O$ has two types of interlayers that are piled up alternately and exhibit different reactivities [48]. Interlayer I possesses hydrated water and shows high reactivity, which anhydrous interlayer II exhibits low reactivity. There have been a certain number of reports of reactions between $K_4Nb_6O_{17}{\cdot}3H_2O$ and organic molecules using the differences in reactivity between interlayer I and interlayer II [33].

Intercalation of small ammonium ions occurred sequentially, first in interlayer I and then in interlayer II [49]. On the other hand, bulky ammonium ions were intercalated only into interlayer I [50]. Compounds that were modified only in interlayer I were called A-type, and compounds that were modified in both interlayers I and II were called B-type. Kimura et al. modified the $K_4Nb_6O_{17}{\cdot}3H_2O$ surfaces with phenylphosphonic acid using A-type and B-type ion-exchanged intercalation compounds of $K_4Nb_6O_{17}{\cdot}3H_2O$ [51]. In their report, bulky dioctadecyldimethylammonium ions were intercalated into only interlayer I, and A-type phenylphosphonate derivatives were obtained using this A-type ammonium intercalation compound as an intermediate. On the other hand, dodecylammonium ions were intercalated into both interlayers I and II and a B-type phenylphosphonate derivative was obtained using this B-type ammonium intercalation compound as an intermediate. Thus, regioselective surface modification of $K_4Nb_6O_{17}{\cdot}3H_2O$ by organophosphonic acid was successfully achieved.

A variety of nanosheets have been obtained by exfoliation of layered materials [52], and various methods have been reported for their exfoliation. A simple method of exfoliation is dispersing layered materials in water. Water molecules can intercalate in the interlayer and promote exfoliation [53]. Bulky ammonium ions intercalated in the interlayer can expand the interlayer distance and decrease interactions between the negative charge and positive charge to cause exfoliation. [54]. Mechanical exfoliation using ultrasonication has also been employed [55]. On the other hand, *in situ* polymerization of organic monomers in the interlayer can also lead to exfoliation of layered materials. A modifier grafted onto the interlayer surface is reacted with monomers and generates polymer chains that expand the interlayer distance. This polymerization method is called the “grafting from” method and is often reported in the field of graphene [56]. Introducing small molecules, such as carboxyl acids, into the interlayer as an initiator group could cause polymerization from the surface of graphene [57, 58]. Another report of the “grafting from” method utilized a layered perovskite, $HLaNb_2O_7{\cdot}xH_2O$, which was modified with organophosphonic acid bearing an initiation group on the interlayer surface, and *N*-isopropylacrylamide (NIPAAm) was polymerized from the initiation group by atom transfer radical polymerization [59]. The interlayer distance was expanded by polymerization, and nanosheets dispersed in water were obtained. Because a thermos-responsive polymer, poly(*N*-isopropylacrylamide), PNIPAAm, was bound to the nanosheet surfaces, the nanosheets were hydrophilic and dispersed in water at below the lower critical solution temperature (LCST). On the contrary, the nanosheets become hydrophobic and aggregate at over the LCST in water.

In this research, the preparation of Janus nanosheets was achieved by taking advantage of the presence of two types of interlayers with different reactivities in $K_4Nb_6O_{17}{\cdot}3H_2O$. Interlayer II of an A-type organophosphonic acid derivative of $K_4Nb_6O_{17}{\cdot}3H_2O$ was reacted with another type of organophosphonic acid. Both sides of niobate nanosheets were modified by two organophosphonic acids regioselectively, because organophosphonic acid could not undergo an exchange reaction and homocondensation. Janus nanosheets could be obtained by exfoliation of the

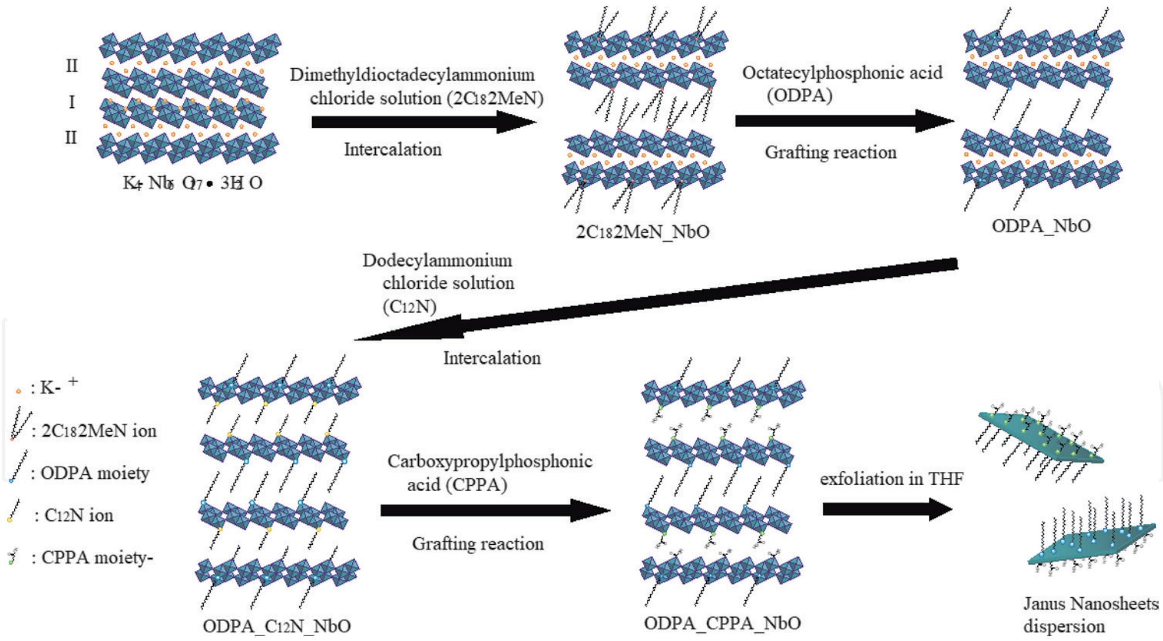

Figure 1.
Preparation of Janus nanosheet.

product into single-layer nanosheets in an appropriate solvent, THF. Lipophilic octadecylphosphonic acid (ODPA) and hydrophilic carboxypropylphosphonic acid (CPPA) were chosen as the organophosphonic acids. The properties of both sides of Janus nanosheets were explored by the AFM phase imaging technique. This report is based on a study first reported in Chemical Communications (**Figure 1**) [60].

2. Experimental section

An A-type alkylammonium intercalation compound, $(2C_{18}2MeN)_{1.0}(K, H)_3[Nb_6O_{17}]$ ($2C_{18}2MeN$ = dioctadecyldimethylammonium ion), was prepared based on the previous report [49]. Octadecylphosphonic acid (ODPA) was synthesized as described elsewhere [61, 62]. Dodecyltrimethylammonium chloride, carboxypropylphosphonic acid (CPPA), 2-butanone, acetone, and tetrahydrofuran (THF) were used without further purification.

First, interlayer I of the A-type alkylammonium intercalation compound was modified by ODPA. The A-type alkylammonium intercalation compound (0.05 g) and ODPA (0.048 g) were used to adjust the Nb:ODPA molar ratio to 1:4 and reacted in 2-butanone (20 mL) at 150°C for 7 days. After the reaction, the crude product was centrifuged, washed with THF and HCl (pH = 3), and air-dried (ODPA_NbO). The cations (K^+, H^+) in interlayer II were then exchanged with the dodecylammonium ion ($C_{12}N^+$) to expand interlayer II. ODPA_NbO (0.1 g) and dodecyltrimethylammonium chloride (0.19 g) were used to adjust the ODPA:$C_{12}N^+$ molar ratio to 1:10 and reacted in water (10 mL) at 80°C for 3 days. After the reaction, the crude product was centrifuged, washed with water, and air-dried (ODPA_C_{12}N_NbO). Then, interlayer II of ODPA_C_{12}N_NbO was modified by CPPA. ODPA_C_{12}N_NbO (0.05 g) and CPPA (0.05 g) were used to adjust the Nb:CPPA molar ratio to 1:10 before reaction in 2-butanone (10 mL) at 80°C for 3 days. After reaction, the crude product was centrifuged, washed with THF and HCl (pH = 3), and corrected as a precipitate (ODPA_CPPA_NbO). After centrifugation, the product dispersed in supernatant was corrected by slow evaporation of THF (ODPA_CPPA_NbO_evaporation). TEM and AFM samples were prepared by stirring ODPA_CPPA_NbO in THF to exfoliate them into single-layer nanosheets.

3. Analysis

XRD analysis (convergence method) was carried out with a Rigaku RINT-1000 diffractometer (Mn-filtered FeKα radiation). XRD analysis (parallel beam method) was performed with a Rigaku SmartLab diffractometer (oblique incidence, FeKα radiation). IR analysis was conducted with a JASCO FT/IR-460 Plus spectrometer by the KBr method. Solid-state ^{31}P magic angle spinning (MAS) NMR spectra were recorded on a JEOL JNM-ECX400 spectrometer. The measurement conditions were as follows: resonance frequency: 160.26 MHz; pulse angle: 90°; pulse delay: 30 s; and MAS frequency: 12 kHz. Triphenylphosphine (−8.4 ppm) was used as a reference. Solid-state ^{13}C cross-polarization (CP)/MAS NMR spectra were recorded on a JEOL JNM-ECX-400 spectrometer. The measurement conditions were as follows: resonance frequency: 99.55 MHz; pulse delay: 5 s; contact time: 1.5 ms; and MAS frequency: 12 kHz. Hexamethylbenzene (17.4 ppm) was used as a reference. ICP-AES measurement was performed using a Thermo Jarrell Ash ICAP-574II instrument. Samples (about 10 mg) were dissolved by heating at 150°C overnight in HF (1 mL), HCl (3 mL), and HNO_3 (4 mL). H_3BO_3 (70 mL) was added as a masking reagent for HF. HF (1 mL), HCl (3 mL), HNO_3 (4 mL), and H_3BO_3 (70 mL) were added to each standard solution for matrix matching. The amounts of C, H, and N in the samples were measured by elemental analysis using a PerkinElmer PE2400II instrument. Transmission electron microscope (TEM) images were observed with a JEOL JEM-1011 microscope operating at 100 kV. A TEM sample was prepared by dropping drops of a dispersion on a Cu 150P grid and drying under reduced pressure. Atomic force microscope (AFM) images were observed with an Agilent 5500 AFM/SPM microscope in the acoustic AC mode under ambient conditions. An ordinary commercial silicon cantilever was used as an AFM tip (e.g., a RTESP-300 from Bruker: resonance frequency ≈ 300 kHz, and spring constant ≈ 40 N/m). Samples for AFM were prepared by spin coating of the dispersion on a Si wafer.

4. Results and discussion

Figure 2 shows ^{13}C CP/MAS NMR spectra of the products. In the spectrum of ODPA_NbO (**Figure 2a**), signals assignable to the octadecyl group were observed. It is likely that the ODPA moiety was introduced into interlayer I, since dioctadecyldimethylammonium ions, whose presence was required for interlayer modification with organophosphonic acids [51], were present only in interlayer I. In the spectrum of ODPA_C_{12}N_NbO (**Figure 2b**), signals assignable to alkyl chains (octadecyl and dodecyl) were observed at 15–43 ppm [51]. In addition, a signal assignable to a carbon atom adjacent to a nitrogen atom was observed at 43 ppm [63], indicating the presence of $C_{12}N^+$. Since $C_{12}N^+$ is known to be intercalated into both interlayer I and interlayer II [48], the intercalation of $C_{12}N^+$ into interlayer II was likely to occur. In the spectrum of ODPA_CPPA_NbO (**Figure 2c**), signals due to alkyl chains were observed at 15–36 ppm. On the other hand, a signal originating from $C_{12}N^+$ at 43 ppm disappeared and a signal due to C=O groups of CPPA was observed at 178 ppm [64]. These results suggest the removal of $C_{12}N^+$ and introduction of the CPPA moiety to ODPA_CPPA_NbO.

Figure 3 shows IR spectra of the products. In the spectrum of ODPA_NbO (**Figure 3a**), absorption bands due to ν (C–H), σ_s (CH_2), and ν (P–O) modes were observed at 2956–2849, 1468, and 1011 cm^{-1}, respectively [65], indicating that ODPA moiety was present in ODPA_NbO. In the spectrum of ODPA_C_{12}N_NbO (**Figure 3b**), an adsorption band at 1540 cm^{-1} assignable to the σ (N–H) mode was observed in addition to the aforementioned adsorption band, indicating that

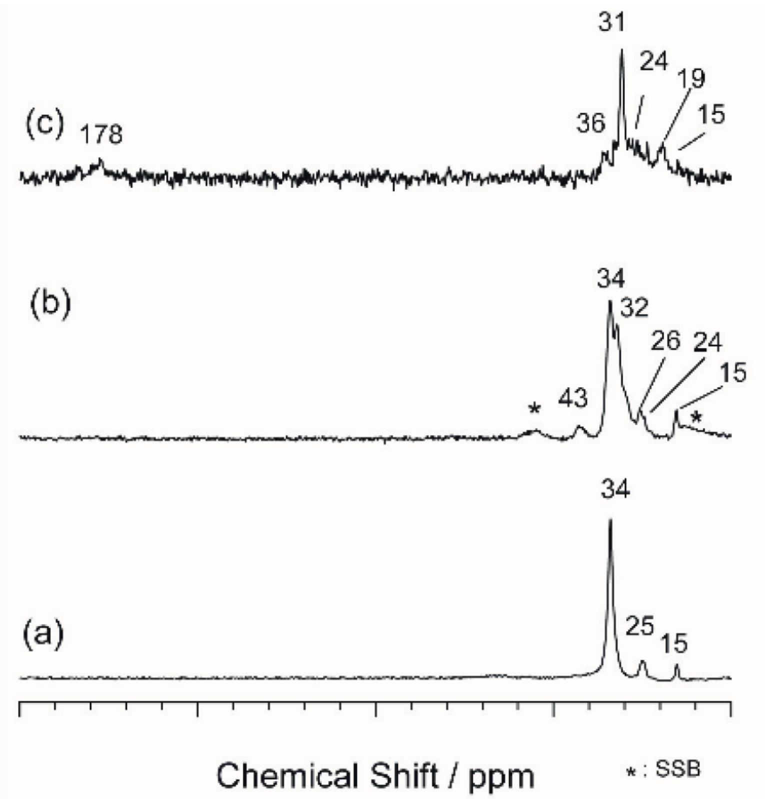

Figure 2.
^{13}C CP/MAS NMR spectra of (a) ODPA_NbO, (b) ODPA_C_{12}N_NbO, and (c) ODPA_CPPA_NbO.

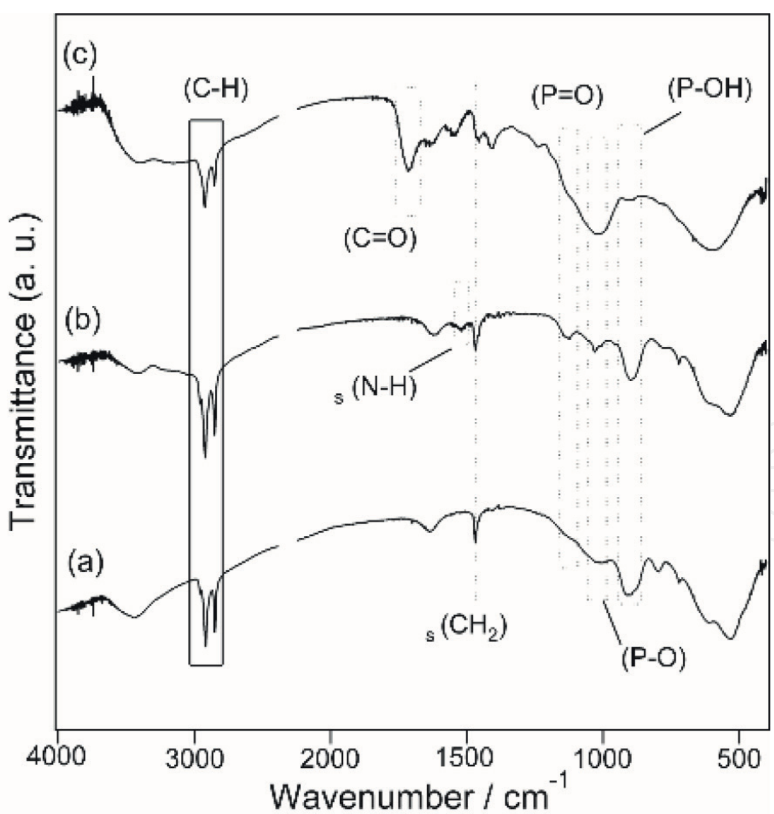

Figure 3.
IR spectra of (a) ODPA_NbO, (b) ODPA_C_{12}N_NbO, and (c) ODPA_CPPA_NbO.

octadecylammonium ions were present in ODPA_C_{12}N_NbO. In the spectrum of ODPA_CPPA_NbO (**Figure 3c**), a new adsorption band that was assignable to the σ (C=O) mode of the CPPA moiety was observed at 1700 cm^{-1} [66], indicating the presence of the CPPA moiety in ODPA_CPPA_NbO. It was reported that an adsorption band due to the ν_{as} (CH_2) of alkyl chain was shifted from 2924.7 cm^{-1} to a lower wavenumber by increasing the packing density of the alkyl chain [67]. In the case of the *all-trans* octadecyl alkyl chain, ν_{as} (CH_2) was observed at 2917.8 cm^{-1} [67, 68] and a σ_s (CH_2) band was observed at 1468 cm^{-1} [68]. In the spectrum of ODPA_NbO, adsorption bands assignable to ν_{as} (CH_2) and ν_s (CH_2) modes were observed at 2918 and 2848 cm^{-1}, respectively, and a σ_s (CH_2) adsorption band was observed at 1468 cm^{-1}. Thus, the alkyl chain in ODPA_NbO was likely to be in an *all-trans* conformation. On the other hand, ν_{as} (CH_2), ν_s (CH_2), and σ_s (CH_2) adsorption bands were observed at 2923, 2852, and 1456 cm^{-1} in the spectrum of ODPA_CPPA_NbO, respectively, indicating that the alkyl chain in ODPA_CPPA_NbO was likely to contain *gauche-blocks*.

Figure 4 shows ^{31}P MAS NMR spectra of the products. A signal was observed at 28 ppm in the spectrum of ODPA_NbO (**Figure 4a**). This signal was shifted upfield from the chemical shift of the ODPA molecule (33 ppm at ^{31}P MAS NMR) by 5 ppm, indicating that interlayer surface modification by ODPA had proceeded and an Nb–O–P bond had been formed [47]. In the spectrum of ODPA_C_{12}N_NbO (**Figure 4b**), a signal was observed at 25 ppm. This signal was shifted upfield from 28 ppm, the chemical shift of ODPA_NbO, by 3 ppm. This shift suggests that $C_{12}N^+$ would change the electronic environment around the P atom by an ion exchange reaction with H^+ of the P–OH group [47], although the details were not yet clarified. Thus, it is likely that $C_{12}N^+$ was intercalated not only in interlayer II, but probably also in interlayer I upon the reaction with ODPA_NbO. In the spectrum of ODPA_CPPA_NbO (**Figure 4c**), a new signal was observed at 31 ppm in addition to the signal at 28 ppm. The signal at 28 ppm was observed in the same position as that of the ODPA moiety of ODPA_NbO, confirming maintenance of the ODPA moiety at interlayer I. Because a signal of a CPPA molecule was observed at 34 ppm, a signal at 31 ppm was assignable to the CPPA moiety. This signal was shifted upfield by 3 ppm, indicating

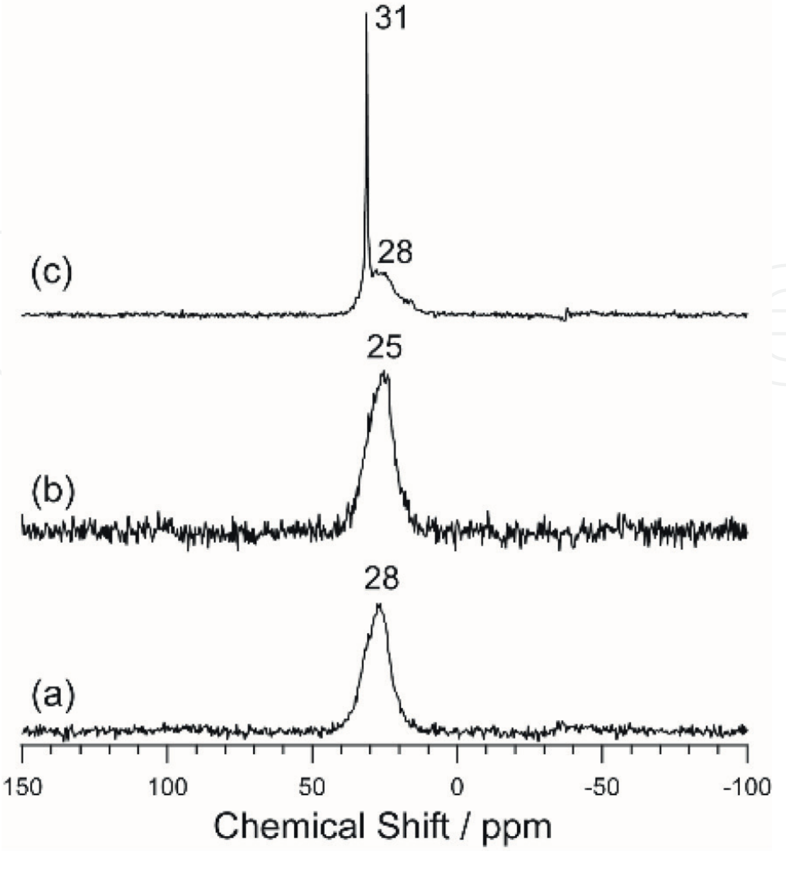

Figure 4.
^{31}P MAS NMR spectra of (a) OPDA_NbO, (b) ODPA_C_{12}N_NbO, and (c) ODPA_CPPA_NbO.

that the CPPA moiety was grafted onto the interlayer surface and a Nb–O–P bond was formed. The above results suggested that ODPA and CPPA formed covalent bonds with the $[Nb_6O_{17}]^{4-}$ sheet surface. Since bands assignable to P–OH groups and P=O groups were observed in the IR spectrum of ODPA_CPPA_NbO, ODPA and CPPA were likely to be in a monodentate environment on the surface of $[Nb_6O_{17}]^{4-}$ sheet.

Table 1 shows the molar ratio calculated from the ICP measurement and elemental analysis. The molar ratio of ODPA_NbO was P:Nb = 1.3:6.0. On the other hand, the molar ratios of ODPA_C_{12}N_NbO and ODPA_CPPA_NbO were P:Nb = 1.3:6.0 and P:Nb = 3.5:6.0, respectively. Intercalation of $C_{12}N^+$ proceeded without release of the ODPA moiety in ODPA_NbO, because the molar ratio of P and Nb of ODPA_NbO did not change after reaction with a dodecylammonium chloride solution. Also, the molar ratio of P to 6 Nb in ODPA_CPPA_NbO increased by 2.2 (3.5 – 1.3), confirming grafting of the CPPA moiety. Assuming Nb = 6.0, the maximum modification amounts for interlayer I and II are 2.0 [51]. Since the Nb–O–P bond was stable with respect to hydrolysis and no homocondensation between two P–OH groups of phosphonic acid occurred under mild conditions [36], the amount of the ODPA moiety in interlayer I was estimated to be 1.3 (65% of the maximum modification amount), that of the CPPA moiety at interlayer I was in the range of 0.2–0.7 (10–35% of maximum modification amount), and that of the CPPA moiety in interlayer II was in the range of 1.5–2.0 (75–100% of the maximum modification amount). Thus, an organic derivative with interlayer I and interlayer II dominantly modified with hydrophobic ODPA and hydrophilic CPPA, respectively, were successfully prepared (**Figure 5**).

Based on the nitrogen ratio of ODPA_NbO, it seems that a small amount of unreacted A-type alkylammonium intercalation compound was present in ODPA_NbO or a small number of released $2C_{18}2MeN$ ions were present in interlayer I *via* ion exchange. Since the amount of K^+ in interlayer II in ODPA_C_{12}N_NbO decreased, an ion exchange reaction between K^+ and H^+ ions at interlayer II and $C_{12}N^+$ proceeded. Because no nitrogen was detected in ODPA_CPPA_NbO, $C_{12}N^+$ was completely removed from interlayer I and II after the reaction with CPPA.

A THF dispersion of nanosheets was easily attained by dispersing ODPA_CPPA_NbO in THF. The resulting dispersion was cast on a TEM grid, and TEM observation was carried out (**Figure 6**). A sheet-like morphology with low contrast was observed. Spots observed in the electron diffraction (ED) pattern can be assigned to 200, 202, and 002 of the orthorhombic cells, and the lattice parameters were calculated to be a = 0.80 nm and c = 0.64 nm. This ED pattern was thus a b-axis incidence pattern of $K_4Nb_6O_{17}$·$3H_2O$ [69]. Based on these results, ODPA_CPPA_NbO was synthesized while maintaining the crystal structure of the $[Nb_6O_{17}]^{4-}$ nanosheets.

Figure 7 shows XRD patterns of the products. The d values of low-angle diffractions due to repeating distances were as follows: the d value of ODPA_NbO, A-type derivative (**Figure 7a**), was 5.67 nm and the d value of ODPA_C_{12}N_NbO (**Figure 7b**) was 4.03 nm. If intercalation of $C_{12}N^+$ into interlayer II proceeded while maintaining an A-type stacking sequence, the d value of ODPA_C_{12}N_NbO is likely to have increased from that of ODPA_NbO. It is possible that a B-type stacking sequence was generated due to exfoliation and restacking during the reaction,

	Nb/–	K/–	P/–	N/–
ODPA_NbO	6.0	2.6	1.3	0.082
ODPA_C_{12}N_NbO	6.0	0.58	1.3	1.8
ODPA_CPPA_NbO	6.0	0.49	3.5	—

Table 1.
Molar ratios of ODPA_NbO, ODPA_C_{12}N_NbO, and ODPA_CPPA_NbO.

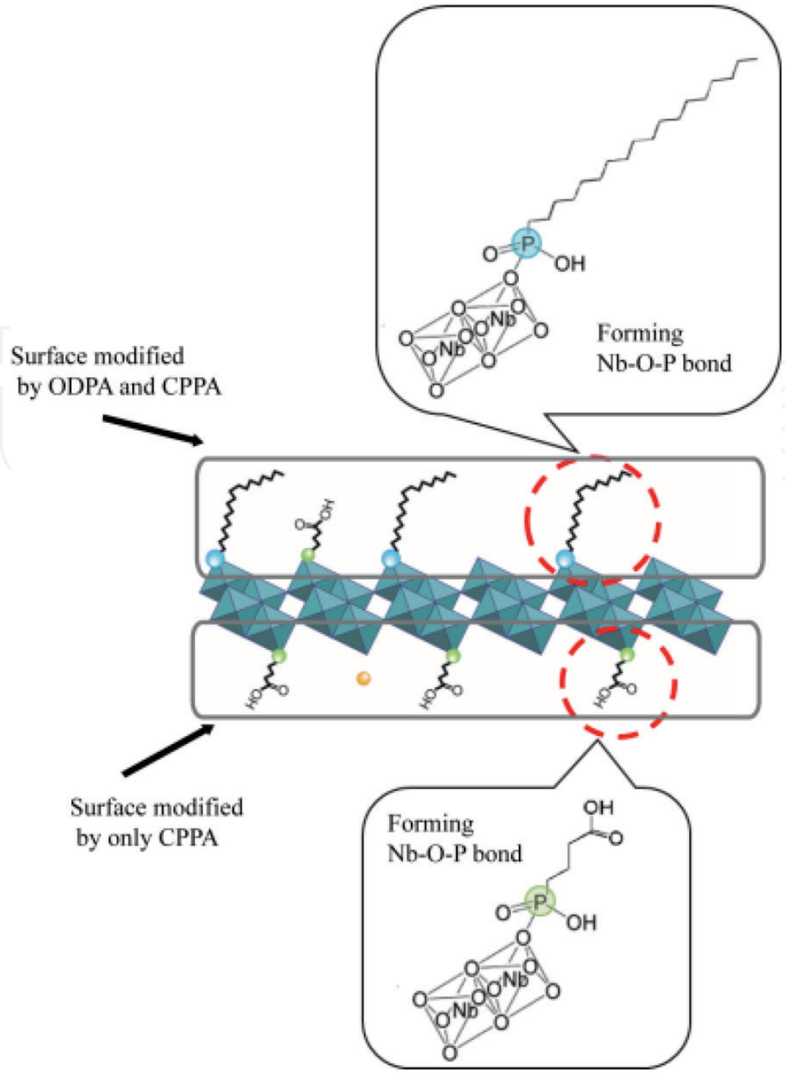

Figure 5.
Proposed structure of ODPA_CPPA_NbO.

resulting in a smaller repeating distance. Also, the *d* values of ODPA_CPPA_NbO (**Figure 7c**) and ODPA_CPPA_NbO_evaporation (**Figure 7d**) were 2.41 and 4.74 nm, respectively. The stacking sequence would therefore be changed by reaction between ODPA_C_{12}N_NbO and CPPA.

Here, the difference between these two *d* values is discussed. If ODPA_CPPA_NbO is a B-type derivative, the thickness of an organic moiety layer (sum of an ODPA monolayer and a CPPA monolayer) can be calculated by subtracting 0.82 nm, the niobate layer thickness, from 2.41 nm to make 1.59 nm [51]. The repeating distance of an A-type derivative could thus be estimated as the sum of a double niobate layer thickness and a double organic layer thickness. The repeating distance of an A-type derivative can therefore be estimated as follows: (1.59 nm × 2) + (0.82 nm × 2) = 4.82 nm. This value is approximately equal to *d* = 4.74 nm of ODPA_CPPA_NbO_evaporation. From these estimations, it is proposed that ODPA_CPPA_NbO is a B-type derivative and ODPA_CPPA_NbO_evaporation is an A-type derivative. As shown in **Figure 8**, a B-type derivative could be generated by forced restacking *via* centrifugation of exfoliated nanosheets (**Figure 8a** and **b**). On the other hand, an A-type derivative, in which hydrophilic groups faced each other and hydrophobic groups faced each other, was obtained by slow evaporation under mild conditions (**Figure 8c**).

The crystallite sizes calculated from diffraction of the repeating distances using Scherrer's formula were 3.67 and 7.71 nm for ODPA_CPPA_NbO and

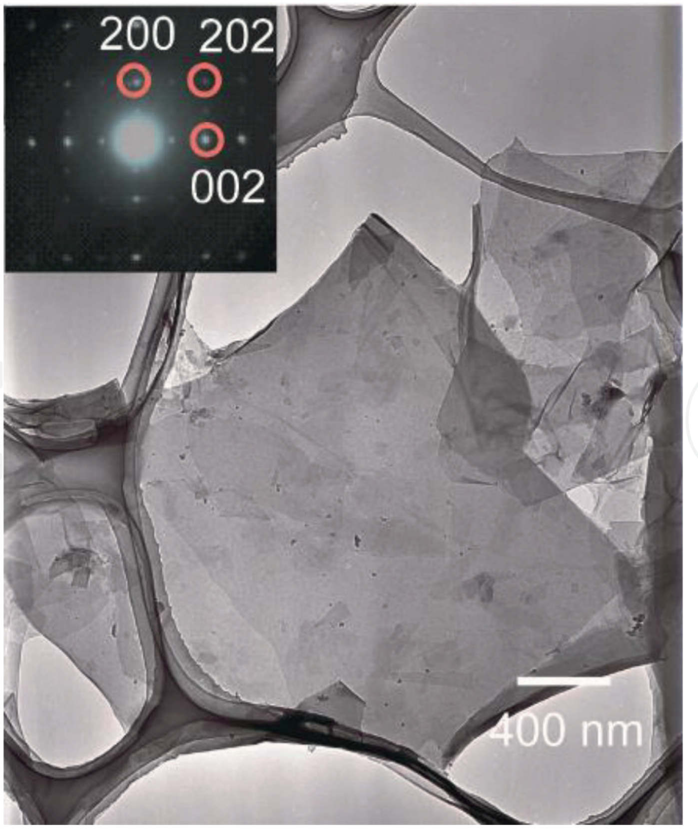

Figure 6.
TEM image of exfoliated ODPA_CPPA_NbO. The inset shows the corresponding ED pattern.

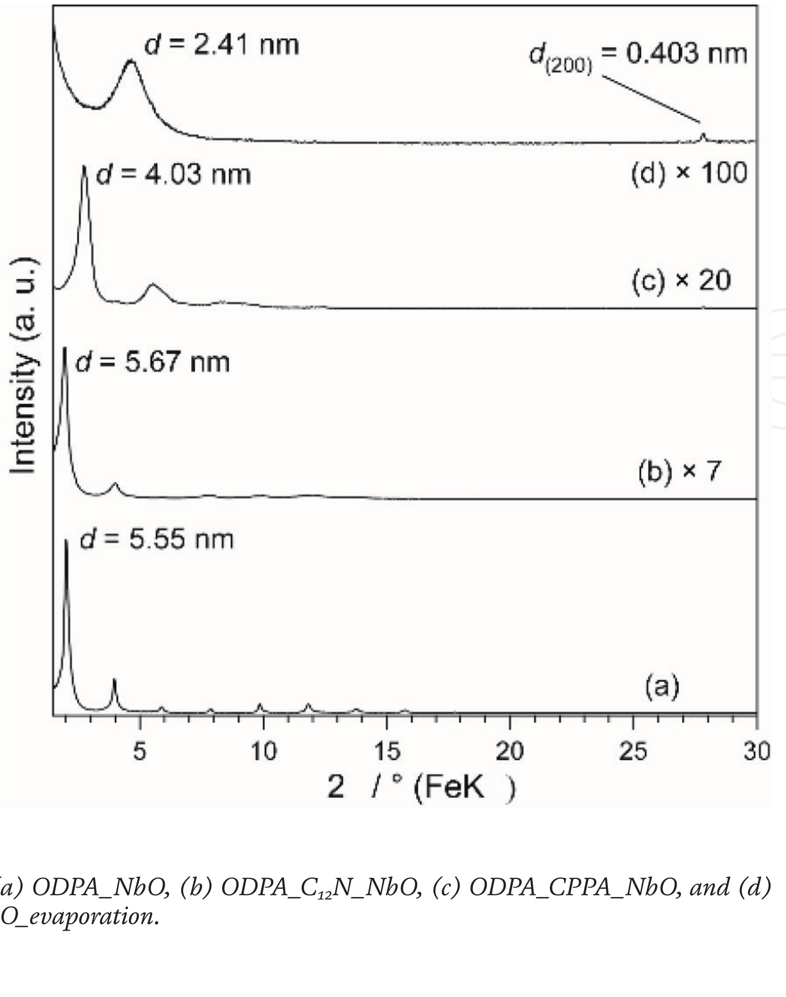

Figure 7.
XRD patterns of (a) ODPA_NbO, (b) ODPA_C_{12}N_NbO, (c) ODPA_CPPA_NbO, and (d) ODPA_CPPA_NbO_evaporation.

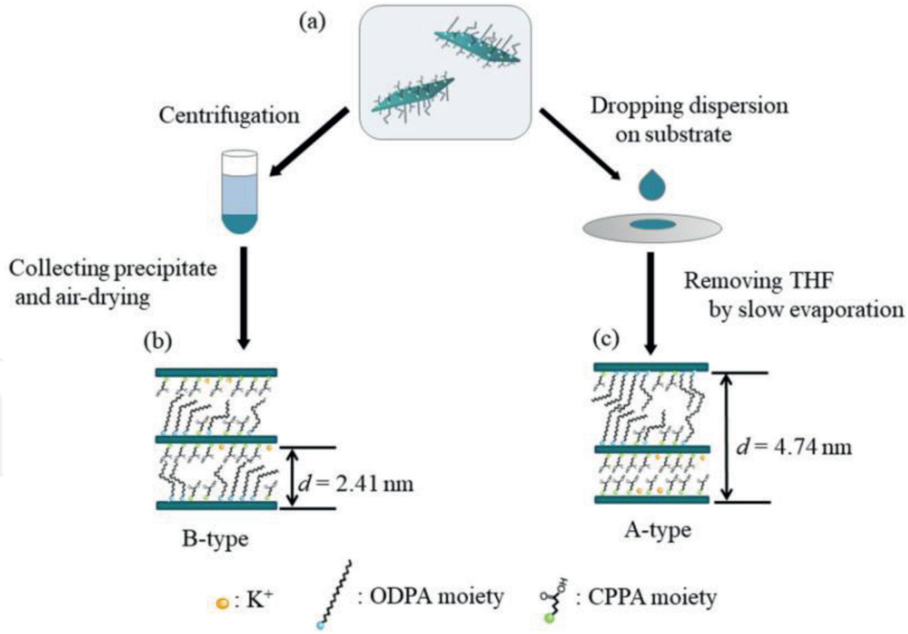

Figure 8.
The estimated structures of ODPA_CPPA_NbO: Possible routes from (a) ODPA_C12N_NbO to (b) ODPA_CPPA_NbO and (c) ODPA_CPPA_NbO_evaporation.

ODPA_CPPA_NbO_evaporation, respectively. The crystallite size of ODPA_CPPA_NbO_evaporation was larger than that of ODPA_CPPA_NbO. It should be noted that underestimation could occur with use of lowest-angle diffractions due to the presence of strain [32]. The crystallite sizes could therefore reflect the average thickness of the particles in the stacking direction, making the number of stacked ODPA_CPPA_NbO nanosheets lower than that of stacked ODPA_CPPA_NbO_evaporation nanosheets. On the other hand, the estimated crystallite size could be interpreted as average thickness of a portion of the stacked sheets with an A-type or B-type stacking sequence. Based on this interpretation, ODPA_CPAN_NbO formed via forced restacking by centrifugation has lower stacking regularity or more random stacking than ODPA_CPPA_NbO_evaporation nanosheets restacked under mild conditions.

Figure 9 shows an AFM image of a sample prepared by spin coating of a THF dispersion of ODPA_CPPA_NbO on a Si wafer. It contained many nanosheets that showed a relatively uniform thickness in the range of 2.5–3.0 nm (**Figure 9A**). This thickness range is approximately equal to the d value of B-type ODPA_CPPA_NbO, indicating that ODPA_CPPA_NbO was exfoliated into single-layer nanosheets that were casted on a Si wafer.

As marked by the a and b arrows in **Figure 9**, two different colored nanosheet surfaces were observed in the phase image (**Figure 9B**). This indicates the presence of two different faces (36–37° and 38–39°) in each Janus nanosheet. This phase difference in the AFM phase image corresponds to the tapping phase gap in the vibration amplitude, and it was reported that the phase difference could occur with a difference in the crystallinity, viscosity, and adhesion of the sample surface [70, 71].

The Janus nanosheets consisted of a hydrophobic surface, which was dominantly covered with the ODPA moiety, and a hydrophilic surface, which was modified with the CPPA moiety. As a result, two chemically different surfaces gave different phases due to differences in the interactions between the apex of the AFM probe and the surfaces of the nanosheets and distinguished visually in the phase image. The origin of the phase contrast would be due to differences in viscosity and hydrophilicity/hydrophobicity. Since the apex of the AFM probe used in this measurement was hydrophilic, it is likely that the high-phase surface and a low-phase surface were assignable to the hydrophilic CPPA moiety and hydrophobic ODPA moiety, respectively.

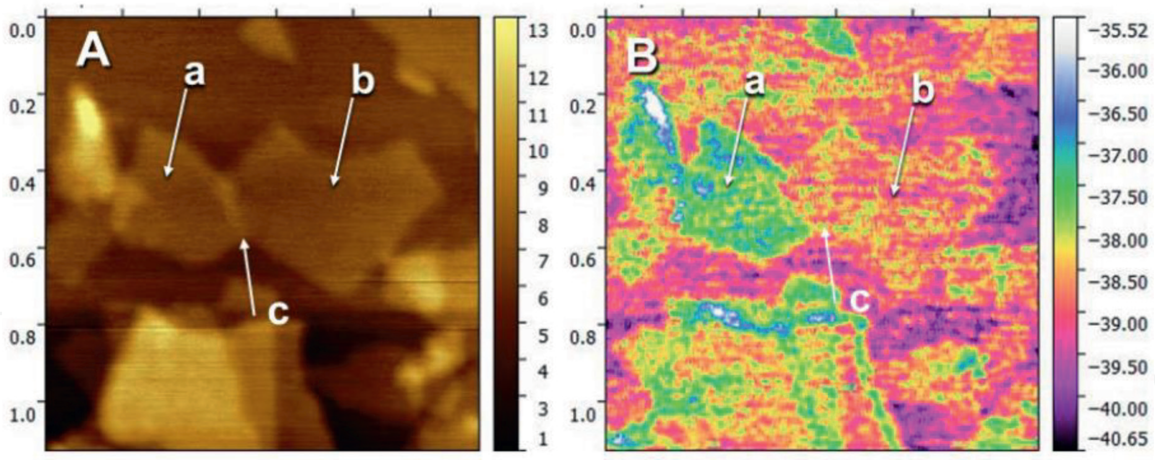

Figure 9.
Topographic (A) and phase (B) AFM images of ODPA_CPPA_NbO Janus nanosheets.

The c arrow in **Figure 9** marks the overlapping area of two nanosheets (a and b). Obviously, these area possessed double-layer thickness. The color of the phase image of this area (**Figure 9B**) indicates that nanosheet b partially overlapped nanosheet a. Thus, these results indicate that hydrophilic and lipophilic surfaces are facing each other. These results also indicate that the nanosheets prepared in this study exhibited hydrophobicity on one side and hydrophilicity on the other.

5. Conclusions

Janus nanosheets were successfully prepared by regioselective and sequential surface modification and exfoliation of $K_4Nb_6O_{17}$·$3H_2O$, whose interlayer I and interlayer II were dominantly modified by ODPA and CPPA, respectively. Since organophosphonic acids bearing various functional groups can be easily synthesized, Janus nanosheet surfaces can exhibit various properties in addition to hydrophobicity and hydrophilicity. The Janus nanosheets prepared by the present method can be dispersed in many solvents, moreover, because organophosphonic moieties are bound to niobate nanosheets by covalent bonds. The Janus nanosheets prepared in this study can be expected to be applied in surface chemistry research because of the hydrophobicity and hydrophilicity on opposing sides of the nanosheets. Also, by changing the functional groups of organophosphonic acids, novel two-dimensional materials with various functions with potential applications in various fields can be realized.

Acknowledgements

This work was financially supported in part by a Grant-in-Aid for Scientific Research on Innovative Areas “New Polymeric Materials Based on Element-Blocks (No. 2401)” (JSPS KAKENHI Grant Numbers JP24102002), “Coordination Asymmetry (JP 23655205),” and Grant-in-Aid for Challenging Exploratory Research (JP17H05378). Reproduced from Ref. [60] with permission from the Royal Society of Chemistry.

Conflict of interest

There are no conflicts to declare.

Author details

Ryoko Suzuki[1], Mitsuhito Sudo[1], Megumi Hirano[2], Naokazu Idota[3], Masashi Kunitake[4], Taisei Nishimi[5] and Yoshiyuki Sugahara[1,6]*

1 Department of Applied Chemistry, School of Advanced Science and Engineering, Waseda University, Tokyo, Japan

2 Technical Division, Faculty of Engineering, Kumamoto University, Kumamoto, Japan

3 Department of Chemical Science and Technology, Faculty of Bioscience and Applied Chemistry, Hosei University, Tokyo, Japan

4 Faculty of Advanced Science and Technology, Kumamoto University, Kumamoto, Japan

5 Japan Technological Research Association of Artificial Photosynthetic Chemical Process (ARPChem), Tokyo, Japan

6 Kagami Memorial Research Institute for Science and Technology, Waseda University, Tokyo, Japan

*Address all correspondence to: ys6546@y.waseda.jp

References

[1] de Gennes PG. Soft matter (Nobel lecture). Angewandte Chemie, International Edition. 1992;**31**:842-845. DOI: 10.1002/anie.199208421

[2] Nishisako T, Torii T, Takahashi T, Takizawa Y. Synthesis of monodisperse bicolored Janus particles with electrical anisotropy using a microfluidic co-flow system. Advanced Materials. 2006;**18**:1152-1156. DOI: 10.1002/adma.200502431

[3] Binks BP, Fletcher PDI. Particles adsorbed at the oil–water Interface: A theoretical comparison between spheres of uniform wettability and "Janus" particles. Langmuir. 2001;**17**:4708-4710. DOI: 10.1021/la0103315

[4] Kim M, Anthony SA, Granick S. Activated surface diffusion in a simple colloid system. Physical Review Letters. 2009;**102**:178303. DOI: 10.1103/PhysRevLett.102.178303

[5] Seo KD, Doh J, Kim DS. One-step microfluidic synthesis of Janus microhydrogels with anisotropic thermo-responsive behavior and organophilic/hydrophilic loading capability. Langmuir. 2013;**29**:15137-15141. DOI: 10.1021/la403015y

[6] Walther A, Muller AHE. Janus particles: Synthesis, self-assembly, physical properties, and applications. Chemical Reviews. 2013;**113**:5194-5261. DOI: 10.1021/cr300089t

[7] Lattuada M, Hatton TA. Synthesis, properties and applications of Janus nanoparticles. Nano Today. 2011;**6**:286-308. DOI: 10.1016/j.nantod.2011.04.008

[8] Jiang S, Chen Q, Tripathy M, Luijten E, Schweizer KS, Granick S. Janus particle synthesis and assembly. Advanced Materials. 2010;**22**:1060-1071. DOI: 10.1002/adma.200904094

[9] Erhardt R, Zhang M, Boker A, Zettl H, Abetz C, Frederik P, et al. Amphiphilic Janus micelles with polystyrene and poly(methacrylic acid) hemispheres. Journal of the American Chemical Society. 2003;**125**:3260-3267. DOI: 10.1021/ja028982q

[10] Qi H, Wang W, Li CY. Janus polymer single crystal nanosheet via evaporative crystallization. ACS Macro Letters. 2014;**3**:675-678. DOI: 10.1021/mz5002806

[11] Perro A, Reculusa S, Pereira F, Delville MH, Mingotaud C, Duguet E, et al. Towards large amounts of Janus nanoparticles through a protection–deprotection route. Chemical Communications. 2005;(44):5542-5543. DOI: 10.1039/B507486J

[12] Hawker CJ. "Living" free radical polymerization: A unique technique for the preparation of controlled macromolecular architectures. Accounts of Chemical Research. 1997;**30**:373-382. DOI: 10.1021/ar960248m

[13] Zhao B, Zhou H, Liu C, Long Y, Yang G, Tungd CH, et al. Fabrication and directed assembly of magnetic Janus rods. New Journal of Chemistry. 2016;**40**:6541-6545. DOI: 10.1039/C6NJ00825A

[14] Oratis AT, Farmer TP, Bird JC. Capillary induced twisting of Janus cylinders. Soft Matter. 2017;**13**:7556-7561. DOI: 10.1039/C7SM01288H

[15] de Leon AC, Rodier BJ, Luo Q, Hemmingsen CM, Wei P, Abbasi K, et al. Distinct chemical and physical properties of Janus nanosheets. ACS Nano. 2017;**11**:7485-7493. DOI: 10.1021/acsnano.7b04020

[16] Stupp SI, Son S, Lin HC, Li LS. Synthesis of two-dimensional polymers. Science. 1993;**259**:59-63. DOI: 10.1126/science.259.5091.59

[17] Walther A, Andre X, Drechsler M, Abetz V, Muller AHE. Janus Discs. Journal of the American Chemical Society. 2007;**129**:6187-6198. DOI: 10.1021/ja068153v

[18] Walther A, Drechsler M, Muller AHE. Structures of amphiphilic Janus discs in aqueous media. Soft Matter. 2009;**5**:385-390. DOI: 10.1039/B812321G

[19] Liang F, Shen K, Qu X, Zhang C, Wang Q, Li J, et al. Inorganic Janus nanosheets. Angewandte Chemie, International Edition. 2011;**50**: 2379-2382. DOI: 10.1002/anie.201007519

[20] Yang H, Liang F, Wang X, Chen Y, Zhang C, Wang Q, et al. Responsive Janus composite nanosheets. Macromolecules. 2013;**46**:2754-2759. DOI: 10.1021/ma400261y

[21] Liu Y, Liang F, Wang Q, Qu X, Yang Z. Flexible responsive Janus nanosheets. Chemical Communications. 2015;**51**:3562-3565. DOI: 10.1039/C4CC08420A

[22] Stçter M, Gçdrich S, Feicht P, Rosenfeldt S, Thurn H, Neubauer JW, et al. Controlled exfoliation of layered silicate heterostructures into bilayers and their conversion into giant Janus platelets. Angewandte Chemie, International Edition. 2016;**55**:7398-7402. DOI: 10.1002/anie.201601611

[23] Ng SW, Noor N, Zheng Z. Graphene-based two-dimensional Janus materials. NPG Asia Materials. 2018;**10**:217-237. DOI: 10.1038/s41427-018-0023-8

[24] Zhang L, Yu J, Yang M, Xie Q, Peng H, Liu Z. Janus graphene from asymmetric two-dimensional chemistry. Nature Communications. 2013;**4**:1443. DOI: 10.1038/ncomms2464

[25] Wu H, Yi W, Chen Z, Wang H, Du Q. Janus graphene oxide nanosheets prepared via Pickering emulsion template. Carbon. 2015;**93**:473-483. DOI: 10.1016/j.carbon.2015.05.083

[26] Osada M, Sasaki T. Exfoliated oxide nanosheets: New solution to nanoelectronics. Journal of Materials Chemistry. 2009;**19**:2503-2511. DOI: 10.1039/B820160A

[27] Joussein E, Petit S, Churchman J, Theng B, Righi D, Delvaux B. Halloysite clay minerals—A review. Clay Minerals. 2005;**40**(04):383-426. DOI: 10.1180/0009855054040180

[28] Madejova J. FTIR techniques in clay mineral studies. Vibrational Spectroscopy. 2003;**31**(1):1-10. DOI: 10.1016/S0924-2031(02)00065-6

[29] Kosuge K, Yamazaki A, Tsunashima A, Otsuka R. Hydrothermal synthesis of magadiite and kenyaite. Journal of the Ceramic Society of Japan. 1992;**100**(3):326-331. DOI: 10.2109/jcersj.100.326

[30] Brindley GW. Unit cell of magadiite in air, in vacuo, and under other conditions. American Mineralogist. 1969;**54**(11-1):1583-1591

[31] Wolf F, Schwieger W. Ion exchange of monovalent cations in synthetic sodium polysilicates with layer structure. Zeitschrift für Anorganische und Allgemeine Chemie. 1979;**457**(1):224-228. DOI: 10.1002/zaac.19794570128

[32] Sasaki T, Watanabe M. Osmotic swelling to exfoliation. Exceptionally high degrees of hydration of a layered titanate. Journal of the American Chemical Society. 1998;**120**(19): 4682-4689. DOI: 10.1021/ja974262l

[33] Bizeto MA, Shiguihara AL, Constantino VRL. Layered niobate nanosheets: Building blocks for advanced materials assembly. Journal of Materials Chemistry. 2009;**19**: 2512-2525. DOI: 10.1039/B821435B

[34] Osada M, Sasaki T. Two-dimensional dielectric nanosheets: Novel nanoelectronics from nanocrystal building blocks. Advanced Materials. 2012;**24**:210-228. DOI: 10.1002/adma.201103241

[35] Guerrero G, Alauzun JG, Granier M, Laurencin D, Mutin PH. Phosphonate coupling molecules for the control of surface/interface properties and the synthesis of nanomaterials. Dalton Transactions. 2013;**42**:12569-12585. DOI: 10.1039/c3dt51193f

[36] Guerrero G, Mutin PH, Vioux A. Anchoring of phosphonate and phosphinate coupling molecules on titania particles. Chemistry of Materials. 2001;**13**:4367-4373. DOI: 10.1021/cm001253u

[37] Takahashi N, Kuroda K. Materials design of layered silicates through covalent modification of interlayer surfaces. Journal of Materials Chemistry. 2011;**21**:14336-14353. DOI: 10.1039/C1JM10460H

[38] Yanagisawa T, Kuroda K, Kato C. Organic derivatives of layered polysilicates. II. Reaction of magadiite and kenyaite with diphenylmethylchlorosilane. Bulletin of the Chemical Society of Japan. 1988;**61**:3743-3745. DOI: 10.1246/bcsj.61.3743

[39] Fujita I, Kuroda K, Ogawa M. Synthesis of interlamellar silylated derivatives of magadiite and the adsorption behavior for aliphatic alcohols. Chemistry of Materials. 2003;**15**:3134-3141. DOI: 10.1021/cm011698y

[40] Mochizuki D, Shimojima A, Kuroda K. Formation of a new crystalline silicate structure by grafting dialkoxysilyl groups on layered octosilicate. Journal of the American Chemical Society. 2002;**124**:12082-12083. DOI: 10.1021/ja027512t

[41] Ide Y, Ogawa M. Surface modification of a layered alkali titanate with organosilanes. Chemical Communications. 2003:1262-1263. DOI: 10.1039/B301222K

[42] Nakato T, Hashimoto S. Dispersion of layered hexaniobate in organic solvents through silylation and liquid crystalline behavior of the colloidal suspension. Chemistry Letters. 2007;**36**:1240-1241. DOI: 10.1246/cl.2007.1240

[43] Mercier L, Facey GA, Detellier C. Organo-layered silicates. Interlamellar intercation and grafting of ethylene glycol in magadiite. Journal of the Chemical Society, Chemical Communications. 1994:2111-2112. DOI: 10.1039/C39940002111

[44] Mitamura Y, Komori Y, Hayashi S, Sugahara Y, Kuroda K. Interlamellar esterification of H-magadiite with aliphatic alcohols. Chemistry of Materials. 2001;**13**:3747-3753. DOI: 10.1021/cm010029h

[45] Tahara S, Ichikawa T, Kajiwara G, Sugahara Y. Reactivity of the Ruddlesden-Popper phase $H_2La_2Ti_3O_{10}$ with organic compounds: Intercalation and grafting reactions. Chemistry of Materials. 2007;**19**:2352-2358. DOI: 10.1021/cm0623662

[46] Asai Y, Ariake Y, Saito H, Idota N, Matsukawa K, Nishino T, et al. Layered perovskite nanosheets bearing fluoroalkoxy groups: Their preparation and application in epoxy-based hybrids. RSC Advances. 2014;**4**:26932-26939. DOI: 10.1039/c4ra01777c

[47] Shimada A, Yoneyama Y, Tahara S, Mutin PH, Sugahara Y. Interlayer surface modification of the protonated ion-exchangeable layered perovskite $HLaNb_2O_7{\cdot}xH_2O$ with organophosphonic acids. Chemistry of Materials. 2009;**21**:4155-4162. DOI: 10.1021/cm900228c

[48] Nakato T, Kuroda K, Kato C. Syntheses of intercalation compounds of layered niobates with methylviologen and their photochemical behavior. Chemistry of Materials. 1992;**4**:128-132. DOI: 10.1021/cm00019a027

[49] Nakato T, Kameyama M, Wei Q, Haga J. Structural response of organically modified layered niobate $K_4Nb_6O_{17}$ to the adsorption of 2,4-dichlorophenol. Microporous and Mesoporous Materials. 2008;**110**:223-231. DOI: 10.1016/j.micromeso.2007.06.011

[50] Wei Q, Nakato T. Competitive adsorption of phenols on organically modified layered hexaniobate $K_4Nb_6O_{17}$. Microporous and Mesoporous Materials. 2006;**96**:84-91. DOI: 10.1016/j.micromeso.2006.06.028

[51] Kimura N, Kato Y, Suzuki R, Shimada A, Tahara S, Nakato T, et al. Single- and double-layered organically modified nanosheets by selective interlayer grafting and exfoliation of layered potassium hexaniobate. Langmuir. 2014;**30**:1169-1175. DOI: 10.1021/la404223x

[52] Nicolosi V, Chhowalla M, Kanatzidis MG, Strano MS, Coleman JN. Liquid exfoliation of layered materials. Science. 2013;**340**(6139):1226400-1226419. DOI: 10.1126/science.1226419

[53] Anderson RL, Ratcliffe I, Greenwell HC, Williams PA, Cliffe S, Coveney PV. Clay swelling—A challenge in the oilfield. Earth Science Reviews. 2010;**98**(3-4):201-216. DOI: 10.1016/j.earscirev.2009.11.003

[54] Ma RZ, Sasaki T. Nanosheets of oxides and hydroxides: Ultimate 2D charge-bearing functional crystallites. Advanced Materials. 2010;**22**(45): 5082-5104. DOI: 10.1002/adma.201001722

[55] Fan X, Xu P, Zhou D, Sun Y, Li YC, Nguyen MAT, et al. Fast and efficient preparation of exfoliated 2H MoS_2 nanosheets by sonication-assisted Lithium intercalation and infrared laser-induced 1T to 2H phase reversion. Nano Letters. 2015;**15**(9):5956-5960. DOI: 10.1021/acs.nanolett.5b02091

[56] Layek RK, Nandi AK. A review on synthesis and properties of polymer functionalized graphene. Polymer. 2013;**54**(19):5087-5103. DOI: 10.1016/j.polymer.2013.06.027

[57] Liu J, Chen C, He C, Zhao J, Yang X, Wang H. Synthesis of graphene peroxide and its application in fabricating super extensible and highly resilient nanocomposite hydrogels. ACS Nano. 2012;**6**:8194-8208. DOI: 10.1021/nn302874v

[58] Fang M, Wang K, Lu H, Yang Y, Nutt S. Single-layer graphene nanosheets with controlled grafting of polymer chains. Journal of Materials Chemistry. 2010;**20**:1982-1992. DOI: 10.1039/B919078C

[59] Idota N, Fukuda S, Tsukahara T, Sugahara Y. Preparation of thermoresponsive nanosheets exhibiting phase transitions in water via surface modification of layered perovskite nanosheets with poly(*N*-isopropylacrylamide) (PNIPAAm). Chemistry Letters. 2015;**44**(2):203-205. DOI: 10.1246/cl.140956

[60] Suzuki R, Sudo M, Hirano M, Idota N, Kunitake M, Nishimi T, et al. Inorganic Janus nanosheets bearing two types of covalently bound organophosphonate groups via regioselective surface modification of $K_4Nb_6O_{17}\cdot 3H_2O$. Chemical Communications. 2018;**54**:5756-5759. DOI: 10.1039/C8CC02892C

[61] Woodward JT, Ulman A, Schwartz DK. Self-assembled monolayer growth of octadecylphosphonic acid on mica.

Langmuir. 1996;**12**:3626-3629. DOI: 10.1021/la9510689

[62] Kim BY, Ratcliff EL, Armstrong NR, Kowalewski T, Pyun J. Ferrocene functional polymer brushes on indium tin oxide *via* surface-initiated atom transfer radical polymerization. Langmuir. 2010;**26**:2083-2092. DOI: 10.1021/la902590u

[63] Mello MR, Phanon D, Silveira GQ, Llewellyn PL, Ronconi CM. Amine-modified MCM-41 mesoporous silica for carbon dioxide capture. Microporous and Mesoporous Materials. 2011;**143**:174-179. DOI: 10.1016/j.micromeso.2011.02.022

[64] Ghosh S, Yu WZ, Kang S, Bhowmik PC, Xing BS. Sorption and fractionation of a peat derived humic acid by kaolinite, montmorillonite, and goethite. Pedosphere. 2009;**19**(1):21-30. DOI: 10.1016/S1002-0160(08)60080-6

[65] Shurvell HF. Spectra-structure correlations in the mid- and far-infrared. In: Chalmers JM, Griffiths PR, editors. Handbook of Vibrational Spectroscopy, Sample Characterization and Spectral Data Processing. Vol. 3. Chichester: John Wiley & Sons; 2002. pp. 1783-1816. DOI: 10.1002/0470027320

[66] Katsumoto Y, Tanaka T, Sato H, Ozaki Y. Conformational change of poly(*N*-isopropylacrylamide) during the coil-globule transition investigated by attenuated total reflection/infrared spectroscopy and density functional theory calculation. The Journal of Physical Chemistry. A. 2002;**106**: 3429-3435. DOI: 10.1021/jp0124903

[67] Quinones R, Rodriguez K, Iuliucci RJ. Investigation of phosphonic acid surface modifications on zinc oxide nanoparticles under ambient conditions. Thin Solid Films. 2014;**565**:155-164. DOI: 10.1016/j.tsf.2014.06.057

[68] Vaia RA, Teukolsky RK, Giannelis EP. Interlayer structure and molecular environment of alkylammonium layered silicates. Chemistry of Materials. 1994;**6**:1017-1022. DOI: 10.1021/cm00043a025

[69] Nassau K, Shiever W, Bernstein JL. Crystal growth and properties of mica-like potassium niobates. Journal of the Electrochemical Society. 1969;**116**:348-353. DOI: 10.1149/1.2411844

[70] Ricci D, Braga C. Imaging methods in atomic force microscopy. In: Ricci D, Braga C, editors. Atomic Force Microscopy Biomedical Methods and Applications. New York City: Humana Press; 2014. DOI: P13-23. DOI:10.1385/1592596479

[71] Magonov SN, Whangbo MH. Phase imaging and stiffness in tapping-mode atomic force microscopy. Surface Science. 1997;**375**:L385-L391. DOI: 10.1016/S0039-6028(96)01591-9